Phosphorylation influences water and ion channel function of AtPIP2;1

Running title: Phosphorylation influences aquaporin ion channel

Jiaen Qiu[1]*, Samantha A. McGaughey[1,2]*‡, Michael Groszmann[2], Stephen D. Tyerman[1], Caitlin S. Byrt[1,2]

*Joint first author

[1]ARC Centre of Excellence in Plant Energy Biology, School of Agriculture, Food and Wine, The University of Adelaide, South Australia, Australia, 5005.

[2]ARC Centre of Excellence for Translational Photosynthesis, Division of Plant Sciences, Research School of Biology, Australian National University, Acton, Australian Capital Territory, Australia, 0200.

‡ Corresponding author: S. McGaughey; Division of Plant Sciences, Research School of Biology, Australian National University, Acton, Australian Capital Territory, Australia, 0200; email: samantha.mcgaughey@anu.edu.au

Abstract

The phosphorylation state of two serine residues within the C-terminal domain of AtPIP2;1 (S280, S283) regulate its plasma membrane localisation in response to salt and osmotic stress. Here we investigated whether the phosphorylation state of S280 and S283 also influence AtPIP2;1 facilitated water and cation transport. A series of single and double S280 and S283 phosphomimic and phosphonull AtPIP2;1 mutants were tested in heterologous systems. In *Xenopus laevis* oocytes, phosphomimic mutants AtPIP2;1 S280D, S283D, and S280D/S283D had significantly greater ion conductance for Na^+ and K^+, whereas the S280A single phosphonull mutant had greater water permeability. We observed a phosphorylation-dependent inverse relationship between AtPIP2;1 water and ion transport with a 10-fold change in both. The results revealed that phosphorylation of S280 and S283 influences the preferential facilitation of ion or water transport by AtPIP2;1. The results also hint that other regulatory sites play roles that are yet to be elucidated. Expression of the AtPIP2;1 phosphorylation mutants in *Saccharomyces cerevisiae* confirmed that phosphorylation influences plasma membrane localisation, and revealed higher Na^+ accumulation for S280A and S283D mutants. Collectively, the results show that phosphorylation in the C-terminal domain of AtPIP2;1 influences its subcellular localisation and cation transport capacity.

Keywords: aquaporin, sodium transport, trafficking, osmotic stress, salt stress, Arabidopsis, potassium, NSCC, regulation, gating

Introduction

Aquaporins are membrane bound channel proteins that facilitate the passive bidirectional movement of water and other small molecules across biological membranes (Chaumont and Tyerman, 2017). Substrates currently known to be transported by aquaporins include gases (O_2; Zwiazek *et al.,* 2017, CO_2; Otto *et al.,* 2010; Uehlein *et al.,* 2003; Uehlein *et al.,* 2012), metalloids (silicon; Ma *et al.,* 2006, boron; Takano *et al.,* 2006, arsenic; Li *et al.,* 2009), reactive oxygen species (H_2O_2; Bienert *et al.,* 2007; Dynowski *et al.,* 2008a; Hooijmaijers *et al.,* 2012; Rodrigues *et al.,* 2017), monovalent ions (Na^+; Byrt *et al.,* 2017; Kourghi *et al.,* 2017; Weaver *et al.,* 1994; NO^-_3; Liu *et al.,* 2020), and other neutral substrates (urea; Dynowski *et al.,* 2008b, glycerol; Gerbeau *et al.,* 1999, ammonia; Loqué *et al.,* 2005). As facilitators of transmembrane water transport, members of the Plasma membrane Intrinsic Protein (PIP) sub-family have roles in mediating water uptake at the root-soil interface, in transcellular water flow, and in regulating hydraulic conductivity in response to abiotic stresses (for reviews see: Chaumont & Tyerman, 2014; Maurel *et al.,* 2015; Gambetta *et al.,* 2017). Similar to some mammalian aquaporin isoforms, a subset of plant PIPs (Arabidopsis PIP2;1 and PIP2;2) were found to facilitate transport of monovalent cations such as Na^+. This activity was more evident at low external calcium and high pH (Byrt *et al.,* 2017; Kourghi *et al.,* 2017). The ability of some plant aquaporins to facilitate Na^+ transport has implications in relation to plant salinity stress responses and tolerance to osmotic stress (McGaughey *et al.,* 2018)

PIP mediated water uptake from soil to roots and changes to root hydraulic conductivity in response to stress (Tournaire-Roux *et al.,* 2002) have been linked to PIP phosphorylation. In Arabidopsis, root hydraulic conductance correlated positively with both protein abundance of PIP2 aquaporins and the abundance of phosphorylated PIP2 proteins (di Pietro *et al.,* 2013).

Exogenous treatment of barley plants with the kinase inhibitor staurosporine significantly reduced root hydraulic conductance (Horie *et al.,* 2011). The phosphorylation states of several conserved serine residues in the cytoplasmic regions of PIPs, including those in the C-terminal domain (CTD), have been implicated in a mechanism where phospho-regulation can directly influence water permeation (Johansson *et al.,* 1998; Törnroth-Horsefield *et al.,* 2006; Nyblom *et al.,* 2009; Yaneff *et al.,* 2016). Phosphorylation of PIPs have also been demonstrated to change in response to salt or osmotic stress thereby influencing PIP trafficking and localisation (Boursiac *et al.,* 2005; Boursiac *et al.,* 2008; Li *et al.,* 2011; Prak *et al.,* 2008). The phosphorylation state of two serine residues in the CTD of AtPIP2;1, S280 and S283, has been reported to change in roots exposed to salt treatments and the phosphorylation of S283 has been associated with the salt-induced internalisation of AtPIP2;1 in Arabidopsis roots (Prak *et al.,* 2008).

In addition to regulating water transport activity of PIPs, phosphorylation may regulate the ion transport activity of plant aquaporins capable of such function. Extensive studies on aquaporin regulation in animals has identified phosphorylation as a key regulator of aquaporin water and ion channel function as well as protein cycling, trafficking, and membrane localisation (Campbell *et al.,* 2012; Eto *et al.,* 2010; Lu *et al.,* 2008; Moeller *et al.,* 2010; Van Balkom *et al.,* 2002; Zhang *et al.,* 2007). Furthermore, the water and ion channel function of soybean (*Glycine max*) NOD-26 (GmNOD-26), the first plant aquaporin to be identified as permeable to both water and ions, was shown to be regulated by phosphorylation of a CTD residue S262 (Guenther *et al.,* 2003; Lee *et al.,* 1995; Weaver *et al.,* 1994). Phosphorylation of S262 altered the voltage sensitivity of GmNOD-26 ion channel activity (Lee *et al.,* 1995) and increased its osmotic water permeability (Guenther *et al.,* 2003). GmNOD-26 phosphorylation was also reported to increase in plants exposed to osmotic stress (Guenther *et al.,* 2003). It is therefore conceivable that phosphorylation could augment

the ability of PIPs to facilitate water and Na^+ transport in isoforms with this dual function. In which case, changes in phosphorylation states would not only regulate PIP protein trafficking and localisation in response to salt and osmotic stresses but also water and Na^+ transport capacity (Byrt *et al.,* 2017; McGaughey *et al.,* 2018).

In this study we investigate the influence of phosphorylation state of two conserved CTD serine residues (S280 and S283) on AtPIP2;1 ion (Na^+ and K^+) and water transport through a series of phosphomimic and phosphonull mutants expressed in heterologous systems. It is important to determine the relationships between PIP protein regulation by phosphorylation and water and ion transport capacity because these features influence plant tolerance to drought and NaCl stresses (McGaughey *et al.,* 2018). Our results indicate that phosphorylation has a key role to play in AtPIP2;1 substrate transport activity where regulation by phosphorylation enables AtPIP2;1 to switch between ion and water channel modes. Given existing information about the regulation of animal aquaporins, and how precisely channel activity, trafficking and localisation are co-ordinately controlled, it is expected that there are similar complexities in the regulation of plant aquaporin function that are yet to be fully explored.

Materials and methods

Cloning, preparation of oocyte constructs and cRNA synthesis

The AtPIP2;1 (At3g53420) coding sequence was cloned using high-fidelity Phusion® polymerase (New England Biolabs, USA) from Arabidopsis root cDNA into a Gateway-enabled pCR8/GW/TOPO entry vector (Life Technologies) before being transferred into the pGEMHE (DEST) vector using LR clonase II (Invitrogen). Primers were designed to

generate site-directed single and double point phosphomimetic mutations in AtPIP2;1 (Table S1) using AtPIP2;1 in pGEMHE as a template. All the constructs in pGEMHE were linearized using restriction enzyme NheI-HF (New England Biolabs, USA) before cRNA was synthesized using mMESSAGE mMACHINE® T7 Transcription kit (Thermo Fisher Scientific, Australia) as previously described Qiu *et al.,* (2016). The concentration and quality of cRNA was determined by NanoDrop and gel electrophoresis.

Preparation of *Xenopus laevis* oocytes

X. laevis oocytes were harvested and stored following Byrt *et al.,* (2017). Oocytes were injected with 46 nL of RNAse-free water using a micro-injector (Nanoinject II, automatic nanolitre injector, Drummond Scientific) with either no cRNA or 23 ng cRNA. Byrt *et al.,* (2017) demonstrated a linear relationship between cRNA concentration and water and ion permeability that saturated at 23 ng. Therefore 23 ng cRNA injections were used in this study. Post injection and prior to experiments oocytes were stored at 18 °C in a Low Na^+ Ringer's solution (62 mM NaCl, 36 mM KCl, 5 mM $MgCl_2$, 0.6 mM $CaCl_2$, 5 mM Hepes, 5% (v/v) horse serum and antibiotics (0.05mg mL^{-1} tetracycline, 100 units mL^{-1} penicillin/0.1 mg mL^{-1} streptomycin)), pH 7.6 for 24-36 h. Expression of AtPIP2;1 within each oocyte batch was confirmed via burst test following Byrt *et al.,* (2017).

Oocyte water permeability

Osmotic water permeability (P_{os}) of oocytes injected with water or cRNA was determined following Byrt *et al.,* (2017) with the following important exception based on the previous finding of rapid Na^+ efflux when the external Na^+ concentration is reduced related to PIP2;1 expression (Byrt *et al.,* 2017): oocytes were pre-incubated in 3 mL iso-osmotic solution (5 mM NaCl, 2 mM KCl, 1 mM $MgCl_2$, 50 μM $CaCl_2$, pH 8.5) with an osmolality of 240 $mosmol.kg^{-1}$ (adjusted with D-mannitol) for 1 h prior to being transferred to a solution with

the same ionic composition (5 mM NaCl, 2 mM KCl, 1 mM $MgCl_2$, 50 μM $CaCl_2$, pH 8.5) with an osmolality of 45 mosmol.kg^{-1} for the photometric swelling assay.

Electrophysiology

Two-electrode voltage clamp (TEVC) recordings were performed on *X. laevis* oocytes 24-36 h post injection. Preparation of glass pipettes was as described in Byrt *et al.,* (2017). TEVC experiments were performed using an Oocyte Clamp OC-725C (Warner Instruments, Hamden, CT, USA) with a Digidata 1440A data acquisition system interface (Axon Instruments, Foster City, CA, USA). Injected oocytes were continuously perfused with solution after being pierced with the voltage and current electrodes and allowed to stabilise. TEVC was performed in solutions consisting of 50 mM NaCl ('Na50'), 100 mM NaCl ('Na100') or 100 mM KCl ('K100') in a basal solution (2 mM KCl, 1 mM $MgCl_2$ and 5 mM HEPES, osmolality was adjusted to 240 mosmol.kg^{-1} with D-mannitol) with 50 μM $CaCl_2$ and pH 8.5. For experiments involving endogenous oocyte kinase stimulation or inhibition, injected oocytes were incubated prior to TEVC in Low Na^+ Ringers (described previously) supplemented with 1 mM 8-Br-cAMP (Sigma (St Louis, MO, USA), #B5386), or 1 mM 8-Br-cGMP (Sigma, #B1381) or 10 μM H7 dihydrochloride (Sigma, #17016) from concentrated stocks dissolved in water. Steady–state currents were recorded starting from –40 mV holding potential for 0.5 s and ranging from 40 mV to –120 mV with 20 mV decrements for 0.5 s before following a –40 mV pulse for another 0.5 s. Ionic conductance was calculated by taking the slope of a regression of the linear region across the reversal potential (–60 mV to +40 mV). TEVC recordings were analysed with CLAMPEX 9.0 software (pClamp 9.0 Molecular Devices, CA, USA).

163 Oocyte Na^+ Content

164 Water control and cRNA injected oocytes were incubated for 24 h in the 'Na100' solution as
165 was used for electrophysiology recordings. Oocytes were removed to individual 1.5 mL
166 microfuge tubes and washed briefly with double distilled H_2O. All solution was removed
167 from the tube and oocytes were stored at –20°C. Oocytes were thawed at room temperature
168 before being homogenised in 0.1 M analytic nitric acid and digested at 42°C for 2 h. Nitric
169 acid digested homogenates were diluted 1:10 with double distilled H_2O, vortexed briefly and
170 centrifuged at 16 000 x g (Beckman Coulter Microfuge® 16) to pellet cell debris. An aliquot
171 of the supernatant was removed for dilution and ion analysis was performed using an Atomic
172 Absorption Spectrophotometer (AAS; Shimadzu AA-7000) according to manufacturer's
173 instructions.

174 Yeast vector cloning and yeast localisation

175 Gateway compatible entry clone containing *AtPIP2;1* was generated in pENTR1a and used as
176 a template to generate site-directed single and double point phosphomimetic mutations in
177 AtPIP2;1 (Table S1). Additional non-stop codon versions of these genes were PCR amplified
178 from the pENTR1a clones with primers containing attB sites and inserted into pZeo using BP
179 clonase (Invitrogen). The pZeo non-stop-codon gene versions were shuttled into pAG426-
180 GPD-eGFP by LR clonase II reaction (Invitrogen) to create C-terminal GFP fusion for sub-
181 cellular protein localisation. The pAG426-GPD-GFP vector which confers strong constitutive
182 transgene expression in yeast, were obtained from Addgene (plasmid #14150) and originally
183 deposited by Susan Lindquist (Alberti *et al.,* 2007). The pAG426-GPD-GFP AtPIP2;1 wild-
184 type and the single and double AtPIP2;1 S280 and S283 phosphorylation mutant constructs
185 were transformed into the Saccharomyces cerevisiae *aqy1/aqy2* double mutant yeast strain
186 (Matα; leu2::hisG; trp1::hisG, his3::hisG; ura352 aqy1D::KanMX aqy2D::KanMX) using

Frozen-EZ Yeast Transformation II kit (Zymo Research). The *aqy1/aqy2* double mutant yeast strain was gifted by Peter Dahl (Hohmann Lab) (Tanghe *et al.,* 2002).

Sub-cellular GFP signal was visualised on a Zeiss LSM780 confocal laser-scanning microscope (Carl Zeiss) operated by Zen Black software and a DIC x40 oil immersion lens. eGFP was excited at 488nm and emission was captured at 495-570nm and RFP was excited at 561nm and emission captured at 580-735, with 24 μm pinhole and master and digital gains identically set for all images and analysis. Between 30 to 160 cells for each of the AtPIP2;1 wild-type and mutant proteins were scored across 3-4 independent experiments with differences in the localisation patterns between the genotypes consistent across sessions. pSM1959 was obtained through Addgene (Susan Michaelis - Addgene plasmid #41837; Metzger *et al.,* 2008).

Yeast Na^+ Content

The full-length cDNA of AtPIP2;1 and AtPIP2;1 single- and double-point C-terminal phosphorylation mutations (Table S1) generated in gateway enabled entry vectors were sub-cloned into pYES-DEST 52 (Invitrogen) yeast expression destination vector driven by *GAL1* promoter through LR reaction. Empty vector and AtPIP2;7 (following Kourghi *et al.,* 2018) were also included as negative controls. Confirmed constructs were transformed into *S. cerevisiae* strain B31 (*Δena1::HIS3::ena4, Δnha1::LEU2*) (Bañuelos *et al.,* 1998) using Frozen-EZ Yeast Transformation II kit (Zymo Research). Successful transformants grown on selective media (Amino acids supplements drop-out without uracil (Sigma), 0.67 % (W/V) Na^+-free Yeast nitrogen base (Formedium), 10 mM MES, 2% glucose (W/V), 2% agar (W/V) and pH 5.6) were inoculated into same liquid media for overnight incubation at 30 °C with shaking. The overnight yeast cultures were diluted to 0.05 at OD_{600nm} before further growing in liquid media containing 2% galactose (W/V) to induce the gene expression in B31 yeast

for 18 h. To test the Na^+ influx, yeast culture were first centrifuged at 2,500 x *g* for 3 min and the supernatant was removed. Yeast cells were then gently resuspended in Na^+ uptake buffer (70 mM NaCl, 10 mM MES, 10 mM EGTA, pH 5.6) and incubated at 30 °C for 40 min before being harvested through a 0.45 µm Millipore filter (Merck). Yeast pellets collected by Millipore filter were washed three times using ice-cold washing buffer (20 mM $MgCl_2$ and D-mannitol to adjust the osmolarity similar to Na^+ uptake buffer). To reduce the potential for uncontrolled ion fluxes across yeast membrane during wash, a running vacuum was connected to the Millipore filter to quickly remove the supernatant and washing buffer. Harvested yeast samples were dried on the Millipore filter at 70 °C for two days and were digested in 1% HNO_3 acid at same temperature for another 2 days. Digested yeast samples were vortexed and centrifuged briefly at 13,000 x g and the supernatant was diluted with MilliQ water. Yeast Na^+ and K^+ contents were measured using Atomic Absorption Spectrophotometer (AAS; Shimadzu AA-7000) according to manufacturer's instructions.

Results

Cyclic nucleotide and kinase inhibitor treatments influence AtPIP2;1 mediated ionic conductance in *X. laevis* oocytes

AtPIP2;1 expression in *X. laevis* oocytes elicits currents in the presence of Na^+ (Byrt *et al.,* 2017). We investigated whether AtPIP2;1-facilitated ion transport may be altered by its phosphorylation state. The activity of endogenous kinases in *X. laevis* oocytes, and hence phosphorylation state of expressed proteins, were manipulated by the exogenous application of membrane permeable cyclic nucleotide monophosphate (cNMP) analogues 8-Br-cAMP and 8-Br-cGMP as kinase stimulators, and the kinase inhibitor H7 (Figure 1). These

pharmacological agents have been used previously in this heterologous system to manipulate kinase activity for testing the functional regulation of mammalian aquaporins by phosphorylation (Campbell *et al.,* 2012; Han and Patil, 2000; Hoffert *et al.,* 2008; Yool *et al.,* 1996).

Oocytes were injected with water or *AtPIP2;1* cRNA and either kept untreated as a control, or incubated in 1 mM 8-Br-cAMP (cAMP) or 8-Br-cGMP (cGMP) for 10 min, or incubated in 10 μM H7 for 2 h, or incubated in H7 prior to a cNMP incubation. The ionic conductance of these oocytes was measured by TEVC (Figure 1). Data was collected from multiple independent oocyte batches; therefore, to remove batch-to-batch variation in native ionic conductance and examine only the response to the treatments the data for treated water injected oocytes were normalised to untreated water injected oocytes (Figure 1a), and treated AtPIP2;1 injected oocytes were normalised to untreated AtPIP2;1 injected oocytes (Figure 1b) within each batch. The representative IV curves of AtPIP2;1 and water injected oocytes are shown in Figure S1.

Water injected oocytes did not respond to any treatment type, with the exception of a slight increase in conductance that was observed upon cGMP treatment (Figure 1a). Incubation of AtPIP2;1 injected oocytes in solutions containing H7 resulted in a significant decrease in ionic conductance relative to untreated (Figure 1b). In contrast, incubation in cAMP increased the ionic conductance of AtPIP2;1 injected oocytes (Figure 1b). AtPIP2;1 injected oocytes that were first incubated in H7 followed by a cAMP incubation had increased ionic conductance compared to those incubated only in H7. This indicates that Na^+ transport facilitated by AtPIP2;1 in oocytes is potentially influenced by phosphorylation status, assuming that the treatments alter endogenous kinase activity that phosphorylate AtPIP2;1. It has previously been demonstrated that *X. laevis* can phosphorylate an expressed PIP2 aquaporin (Johansson *et al.,* 1998).

260 Phosphomimic and phosphonull AtPIP2;1 mutants had altered ionic conductance and Na^+
261 accumulation in *X. laevis* oocytes

262 The phosphorylation state of AtPIP2;1 CTD residues S280 and S283 is altered *in planta* by
263 salt treatments (Prak *et al.,* 2008). To explore the potential regulatory roles of S280 and S283
264 phosphorylation on AtPIP2;1-facilitated ion transport, single and double S280 and S283
265 phosphomimics mutated to aspartic acid (D) or phosphonull mutated to alanine (A) versions
266 of AtPIP2;1 were generated. The ionic conductance of oocytes expressing AtPIP2;1 wild-
267 type (WT) or AtPIP2;1 phosphomimic (S280D, S283D) and phosphonull (S280A, S283A)
268 single and double mutants in the presences of Na^+ and K^+ were measured by TEVC (Figure 2,
269 Figure S2).

270 In the 'Na100' solution the single and double phosphonull mutants S280A, S283A and A/A
271 induced currents and had ionic conductance of similar magnitude to that of AtPIP2;1 WT
272 (Figure 2a-d). Whereas, the expression of the single phosphomimic mutants S280D and
273 S283D and the double phosphomimic mutants D/A, A/D and D/D induced greater currents
274 and ionic conductance than WT or the phosphonull mutants (Figure 2a-d).

275 AtPIP2;1 WT was also able to elicit somewhat larger currents and conductances (20-30%
276 larger) with K^+ as the major univalent cation (Figure 2a,c). The phosphorylation mutants had
277 similar effects on conductance in a 'K100' solution to that observed in the 'Na100' solution.
278 The phosphomimics S280D and S283D had greater ionic conductance than either AtPIP2;1
279 WT or the phosphonull mutants (Figure 2c).

280 The total Na^+ content of AtPIP2;1 WT and phospho-mutant expressing oocytes after 24 h
281 incubation in 'Na100' solution was determined (Figure 2e). Consistent with the trends
282 observed for ionic conductance in the same solution ('Na100'; Figure 2c,d), the
283 phosphomimic single (S280D and S283D) and double mutants (A/D, D/A, D/D) accumulated

greater Na^+ per oocyte than WT (Figure 2e). The phosphonull mutants (S280A, A/A) accumulated similar Na^+ to AtPIP2;1 WT oocytes with the exception of S283A, which had significantly higher Na^+ accumulation and an opposite trend to that observed for ionic conductance (Figure 2a,c,e).

Relationship between phosphorylation, water permeability and ionic conductance of AtPIP2;1

Phosphomimic and phosphonull AtPIP2;1 mutants of CTD sites S280 and S283 differed in their osmotic water permeability (P_{os}) and ionic conductance when expressed in oocytes (Figure 2, Figure S2, Figure 3, Figure S3 and Figure S4). For each individual oocyte included in the experiment, measurements of both P_{os} and ionic conductance were captured so that the relationship between P_{os} and ionic conductance could be investigated.

The P_{os} of oocytes expressing AtPIP2;1 WT, and AtPIP2;1 S280 and S283 single and double phosphomimic and -phosphonull mutants was determined via the photometric swelling assay (Figure S4). The single phosphonull mutant S280A had greater mean P_{os} relative to AtPIP2;1 WT (Figure S4) whereas the double phosphomimic mutants D/A, A/D and D/D all had lower mean P_{os} compared to AtPIP2;1 WT (Figure S4). The lower P_{os} for the D/A and A/D mutants indicates that when either of the S280 or S283 sites are phosphorylated it likely has a dominant effect over the dephosphorylated state of the other site.

To test for a relationship between P_{os}, ionic conductance and CTD phosphorylation state, TEVC was first performed followed by swelling assays on the same oocytes after a 2 h recovery incubation. Data was collected from multiple independent oocyte batches. Individual conductance was plotted against the corresponding P_{os} for each oocyte (Figure S3). For WT and D/D, ionic conductance and P_{os} showed a clear and significant inverse

correlation (Figure S3). A significant inverse linear regression was also observed when all genotypes were combined (Figure S3). To better illustrate the relationship, all data points were binned on the basis of ionic conductance (10 μS bins) regardless of genotype (Figure 3a). The negative correlation between P_{os} and ionic conductance was best fit to a single exponential decay ($p < 0.005$) (Figure 3a) such that a high ionic conductance corresponded to a lower P_{os} similar in level to that of water injected controls (dashed horizontal blue line in Figure 3b). This indicates that phosphorylation at AtPIP2;1 CTD affects ion and water permeability in a reciprocal but variable manner. At the maximum ionic conductance the P_{os} of PIP2;1 is effectively zero, and when P_{os} was maximal the ionic conductance of PIP2;1 expressing oocytes was effectively reduced to zero (i.e. similar to water injected control oocytes; dashed vertical red line Figure 3a and c).

To illustrate the trend with the different CTD phosphomimics and nulls, the frequency distributions are shown for decreasing P_{os} (Figure 3b) and increasing ion conductance (Figure 3c). The red (vertical) and blue (horizontal) dashed lines indicate the means of ionic conductance and P_{os} respectively for H_2O injected oocytes (Figure 3a, b, c). AtPIP2;1 A/A, S283A, A/D and S280D mutants follow the same relative order for the change in mean P_{os} and ionic conductance (Figure 3d).

The frequency distribution of ion and water transport activity was dependent on the phosphorylation mutation. The AtPIP2;1 single and double phosphorylation mutants with at least one phosphomimic residue (S280D, S283D, A/D, D/A, D/D) had greater mean ionic conductance and reduced mean P_{os} relative to AtPIP2;1 WT (Figure 3b, c). The S280D, S283D and D/D mutants exhibited increased frequency of a clustered population with significantly down-regulated P_{os}, in contrast to AtPIP2;1 WT and other mutants that showed a wide distribution of P_{os} (Figure 3b). The different distribution patterns observed in ionic

conductance and P_{os} for the S280 and S283 phosphorylation mimics suggests that other factors or AtPIP2;1 phosphorylation sites may be altered in oocytes.

Phosphomimic and phosphonull AtPIP2;1 mutants had altered Na^+ accumulation in *S. cerevisiae* strain B31

To test whether mimicking AtPIP2;1 C-terminal phosphorylation states influenced cell Na^+ accumulation in yeast, the phosphomimic and phosphonull mutants were expressed in a Na^+ efflux compromised strain B31 (*Δena1::HIS3::ena4, Δnha1::LEU2*). This strain is deficient in Na^+ efflux (Bañuelos *et al.,* 1998) enabling greater potential to distinguish differences in intracellular Na^+ accumulation associated with Na^+ uptake through plasma membrane localised Na^+ transporters under salt treatment. Na^+ accumulation in B31 yeast expressing phosphomimic and phosphonull AtPIP2;1 mutants was measured after the yeast had been incubated in a 70 mM NaCl uptake buffer for 40 min. No significant differences in yeast cell sodium content were observed in the samples prior to the incubation in the NaCl uptake buffer (Figure S5a).

Yeast expressing AtPIP2;1 WT accumulated greater Na^+ than the empty vector control and AtPIP2;7 (Figure 4). AtPIP2;7, an efficient water channel, was used as an additional control as this PIP was previously reported to lack Na^+ induced currents when expressed in *X. laevis* oocytes (Kourghi *et al.,* 2017). Comparison of Na^+ accumulation for yeast expressing each of the single and double phosphomimic and phosphonull mutants of interest, showed that only yeast expressing AtPIP2;1 S280A and S283D accumulated significantly more Na^+ than the empty vector controls (Figure 4). However, mimicking single phosphorylation and de-phosphorylation mutations at S280 and S283 sites influenced Na^+ accumulation (Figure 4). Yeast expressing AtPIP2;1 S280A accumulated significantly greater Na^+ than S280D.

Whereas greater Na^+ accumulation was observed for S283D relative to S283A (Figure 4). In the case of A/D and D/A, although yeast expressing both double mutants had Na^+ contents not significantly different to the empty vector control, A/D caused significantly greater Na^+ accumulation than D/A (Figure 4). Interestingly, when both CTD sites were mimicked in either a phosphorylated or de-phosphorylated state, (D/D and A/A), a similar level of Na^+ accumulation was observed not significantly different to that of empty vector controls (Figure 4).

AtPIP2;1 WT and CTD mutants were capable of facilitating K^+ transport in *X. laevis* oocytes (Figure 2a and c). To examine whether similar trends occur when the proteins of interest were expressed in yeast, the K^+ contents of yeast samples were examined. Prior to the incubation in the NaCl uptake buffer there were no significant differences observed between genotypes (Figure S5b). This was also the case after incubation in the 70 mM NaCl buffer solution for 40 min (Figure S6).

Phosphorylation state of S280 and S283 influences AtPIP2;1 localisation in yeast

Phospho-mutants of CTD sites of AtPIP2;1 not only altered Na^+, K^+ and H_2O conductance in *X. laevis* oocytes (Figure 2 and 3), but also influenced the sub-cellular localisation of AtPIP2;1 in the *S.cerevisiae aqy1/aqy2* double mutant yeast strain (Figure 5). Sub-cellular localisation tendencies of the *AtPIP2;1* phospho-mutants were monitored in yeast using both N- or C-terminal GFP fusions. Fusion of AtPIP2;1 wild-type or AtPIP2;1 phospho-mutants to GFP, redirected GFP from a diffuse cytosolic pattern (Figure 5a) to a predominantly sharp ring around the cell perimeter coinciding with the plasma membrane (PM; Figure 5c-i). Weaker GFP signal associated with the tonoplast of the vacuole was also frequently observed. In addition, a proportion of cells showed internal and patchy perimeter GFP signal,

matching the localisation pattern of the SEC63::RFP endoplasmic reticulum (ER) marker (Figure 5b). The detectable frequency and intensity of the ER co-localisation differed between the AtPIP2;1 wild-type and some of the AtPIP2;1 280/283 phosphomimic mutants (Figure 5j). A difference was observed for the AtPIP2;1 S280D mutant, which had frequently occurring intense GFP signal co-localising to the ER (Figure 5d, e and j), relative to the trend observed for the AtPIP2;1 S283D and AtPIP2;1 D/D mutants, which had distinct GFP signal around the perimeter consistent with PM localisation, and less frequent or intense ER co-localisation (Figure 5f, g, h and j). The tendency of the AtPIP2;1 S280A and A/D mutants to co-localise to the ER was more likely than for wild-type (Figure 5i and j). GFP localisation patterns for the phosphonull AtPIP2;1 S283A and A/A mutants along with the D/A mutant were equivalent to that of wild-type AtPIP2;1 (Figure 5j). There was no discernible difference in the localisation patterning whether the GFP was fused to the N- or C- terminal (data not shown).

Comparisons between the phospho-mutants reveal co-ordinated effects of positions S280 and S283 in determining sub-cellular localisation. The more prominent PM targeting of the AtPIP2;1 D/D mutant in comparison to the A/A, D/A, or A/D mutants, indicates that mimicking of phosphorylation of both S280 and S283 was required to promote a more distinct PM localisation (Figure 5j). The distinct ER co-localisation of AtPIP2;1 S280D was not observed in either of the two other S280D phosphomimic mutants (D/A or D/D) (Figure 5j), indicating that a serine at position 283 could be specifically required in combination with the phosphomimic aspartic acid at position 280 to achieve the distinct ER co-localisation.

Discussion

The AtPIP2;1 homotetramer is able to facilitate water and monovalent cation transport activity *in vivo*, with the phosphorylation states of CTD residues S280 and S283 regulating a switch between ion and water channel functions (Figures 1-4).

Endogenous oocyte kinases have been previously shown to alter plant aquaporin phosphorylation state and influence their water channel activity (Maurel *et al.,* 1995; Van Wilder *et al.,* 2008). Using treatments associated with the stimulation (cNMPs) or inhibition (H7) of the endogenous kinase activity of *X. laevis* oocytes (Glass and Krebs, 1980; Kuwahara *et al.,* 1995), we showed that phosphorylation changes also influences AtPIP2;1 Na^+ transport activity (Figure 1). The ionic conductance of AtPIP2;1 expressing oocytes increased in response to cAMP treatment, and decreased in response to both cGMP and H7 treatment (Figure 1). H7 treatment similarly reduced aquaporin-associated ionic conductance for HsAQP1 expressing oocytes by inhibiting the influence of cAMP on endogenous kinases (Yool *et al.,* 1996). Since different kinases respond to cAMP verses cGMP signalling (Conti *et al.,* 2012) and have different target motifs (Francis and Corbin, 1999), the response of AtPIP2;1-faciliated ionic conductance to cNMP treatments indicates that multiple phosphorylation sites on AtPIP2;1, such as candidate sites in the CTD, may be involved in regulating AtPIP2;1-facilitated ionic conductance and that these sites on AtPIP2;1 are targeted by endogenous oocyte kinases. A direct effect of cNMPs on AtPIP2;1 may also be possible; HsAQP1 ion channel function is activated by direct cGMP binding to its loop D in a phosphorylation-dependent manner (Anthony *et al.,* 2000; Campbell *et al.,* 2012) although an equivalent site is not present in AtPIP2;1.

Previous research revealed that phosphorylation of AtPIP2;1 S280 and S283 changes in response to osmotic stress, such as salinity, and that changes in phosphorylation of these sites influences hydraulics in Arabidopsis (Li *et al.,* 2011; Prado and Maurel, 2013; Prak *et al.,* 2008). In *X. laevis* oocytes, S280 and S283 phosphorylation mutants influenced the transport function of AtPIP2;1, such that relatively greater water transport occurred in phosphonull mutants and greater Na^+ and K^+ transport occurred in phosphomimic mutants (Figure 2 and 3). A phosphorylation-dependent negative relationship was observed for AtPIP2;1-facilitated water transport relative to ion transport (Figure 3 and Figure S3, S4), and an approximately ten-fold change in both permeabilities could be observed between oocytes (Figure S3). When phosphorylation of at least one site was mimicked, the functional effect of that phosphomimic was dominant over the effect of the phosphonull site. For example, both the 280/283 D/A and A/D phospho-mutants had water and ion transport more similar to that of the D/D mutants than the A/A mutants (Figure 2 and 3). Functional dominance and hierarchy among CTD phosphorylation events has been previously reported for the Rattus AQP2 in renal epithelial cells in response to vasopressin. Phosphorylation for some sites does not occur unless the phosphorylation of another site has preceded it (Hoffert *et al.,* 2008) and the effect of phosphorylation of one residue determined channel function and trafficking (Table S2) (Lu *et al.,* 2008). The approximately ten-fold variance seen for the ionic conductance and P_{os} of the D/D mutant suggests that there are likely to be other additional regulatory sites that were not controlled for in these experiments. Further research is needed to test how many other AtPIP2;1 regulatory sites influence water and ion transport functions and explore whether these sites have any sort of dependence on the status of the CTD phosphorylation sites (see Fig 4 of Groszmann *et al.,* 2017)

Greater ionic conductance in the presence of Na^+ and K^+ and greater intracellular Na^+ accumulation were consistently observed for the phosphomimic mutants relative to

phosphonull in oocytes, regardless of which CTD site was mimicking a phosphorylated state. However, the trends for Na^+ accumulation in yeast expressing these mutants differed. Only the yeast expressing the single AtPIP2;1 phosphomimic mutants S280A and S283D were observed to have significantly increased net Na^+ accumulation compared to the empty vector control (Figure 4). The results indicate that different S280 and S283 phosphorylation states might have different effects on facilitating Na^+ flux through AtPIP2;1 in yeast relative to oocytes or could be related to differences between single cell sampling in oocytes versus population mean sampling in yeast. These effects may be further complicated by biological differences between oocyte and yeast cells, such as the absence of a vacuole in oocytes, and associated differences in signalling and regulatory processes involving distinct sets of protein kinases. In oocytes, single phosphomimic mutants S280D and S283D had variation in ionic conductance values ranging from magnitudes similar to that of water injected controls (21 μS and 12 μS) up to the maximum ion conductance observed (177 μS and 200 μS) (Figure 3d). This indicates that other variable factors were influencing ionic conductance and could possibly be associated with differential phosphorylation of another site. Further research is required to test whether another site is variably phosphorylated in oocytes that reduces ion conductance, and whether alternative sites are differentially phosphorylated in yeast.

The phosphorylation status of S280 and S283 was also found to influence the distribution of AtPIP2;1 between the ER and PM in yeast (Figure 5) with different trends depending on the status of S280 relative to S283. Phosphorylation of S280 promoted ER retention of AtPIP2;1 demonstrated by more consistent localisation of the S280D phosphomimic mutant to the ER rather than PM. However, the localisation trend could not be replicated in either the D/A or D/D double mutant, suggesting that a serine residue specifically at S283 is required to exert this function. The single S283D and double D/D phosphomimic mutants localised strongly to the PM (Figure 5j) indicating that phosphorylation of S283 promotes PM localisation in

yeast. This corresponds with reports *in planta*, where correct trafficking of AtPIP2;1 to, and subsequent removal from, the PM is reportedly dependent on phosphorylated or unphosphorylated S283, respectively (Prak *et al.,* 2008). Interestingly, this phosphorylation regulated location cycling was observed in response to NaCl treatment in Arabidopsis roots (Boursiac *et al.,* 2005; Li *et al.,* 2011; Luu *et al.,* 2012; Prak *et al.,* 2008; Ueda *et al.,* 2016) linking changes to AtPIP2;1 CTD phosphorylation, subcellular trafficking, and now ion transport capacity, to a salt stress response. Although changes to subcellular localisation can impact transport capacity, our combined results demonstrate that subcellular trafficking and the switch between ion and water transport are two distinct effects of phosphorylation on AtPIP2;1. For example, the D/A and A/D phosphomimic mutants (Figure 5) have a much greater ionic conductance than the double phosphonull A/A mutant when expressed in *X. laevis* oocytes (Figure 2), despite all three variants having similar subcellular distribution trends. This data, alongside the observation of increased P_{os} of A/A relative to the other mutants (Figure 3), indicates that a mis-localisation of the A/A mutant in oocytes is unlikely to be the cause of its lower ionic conductance. Furthermore, the fact we could make these observations in yeast using an aquaporin from the distant taxa of plants, and that similar mechanisms have been reported for animal aquaporins (see Table S2), indicates the potential for there to have been a shared evolutionary origin for the process of CTD phosphorylation influencing aquaporin function and trafficking.

Several plant General Regulatory Factors (GRFs; also known as 14-3-3 proteins) were recently reported to interact preferentially with AtPIP2;1 when the S280 and S283 sites were phosphorylated. Co-expression of AtPIP2;1 D/D mutant with GRFs 3,4 and 10 in oocytes increased their P_{os} compared to AtPIP2;1 A/A (Prado *et al.,* 2019). In the current study it cannot be excluded that AtPIP2;1 could have interacted with an endogenous oocyte GRF protein, or an endogenous aquaporin-interacting ion channel but this is unlikely. The trends

observed for AtPIP2;1 CTD status and associated ionic conductance do not appear common to all aquaporins. There are conserved CTD phosphorylation sites among some Arabidopsis PIPs, but not all PIPs with these conserved phosphorylation sites confer ionic conductance in oocytes. For example, in Arabidopsis AtPIP2;1, AtPIP2;2, AtPIP2;3, AtPIP2;4 and AtPIP2;7 were found to be unphosphorylated, singly phosphorylated at S280 or diphosphorylated at S280 and S283 (Prak *et al.,* 2008), but AtPIP2;7 did not facilitate ion transport when expressed in oocytes despite having equivalent water transport capacity as AtPIP2;1 (Kourghi *et al.,* 2017). Expression of AtPIP2;7 did not increase Na^+ uptake into yeast either (Figure 4). There is precedent for plant aquaporins having ion channel function that is regulated by CTD phosphorylation in the absence of any interacting partners (Table S2). The soybean (*Glycine max*) Gm-NOD26, produced ion channel activity when reconstituted in lipid bilayers (Weaver *et al.,* 1994) and the water and ion channel function of Gm-NOD26 was regulated by the phosphorylation of CTD residue S262 (Guenther *et al.,* 2003; Lee *et al.,* 1995).

The exact physiological role of dual water and ion transporting aquaporins in plants remains unknown and may differ between tissues (McGaughey *et al.,* 2018). When Arabidopsis roots were exposed to 100 mM NaCl the abundance of the S280/S283 diphosphorylated form decreased (Prak *et al.,* 2008). Since phosphorylation of S280 and S283 increases AtPIP2;1 ion channel function, this reduction in S280/S283 diphosphorylated AtPIP2;1 may be a mechanism, in addition to removal from the PM, to reduce Na^+ influx (and possibly K^+ efflux) under salt stress. Complex relationships between localisation and water-ion transport function have been described for HsAQP1. Polarised distribution of and coordinated water and ion transport through HsAQP1 enables rapid localised changes in cell volume and has been implicated as a key mechanism in cancer cell migration and metastasis (De Ieso and Yool, 2018; Kourghi *et al.,* 2015). A sophisticated relationship between AtPIP2;1 phosphorylation state and AtPIP2;1 trafficking, localisation, and water and ion transport

function may be part of a mechanism for rapidly, reversibly and co-ordinately adjusting water and Na^+ or K^+ flux into or out of the cell under salt and osmotic stress.

Byrt *et al.,* (2017), McGaughey *et al.,* (2018), and Munns *et al.,* (2020) have proposed that AtPIP2;1 and AtPIP2;2 could be molecular candidates for the elusive non-selective cation channels (NSCC) observed *in planta* (Demidchik *et al.,* 2002; Essah *et al.,* 2003; Roberts and Tester, 1997). AtPIP2;1 facilitated the transport of K^+ and similar trends were observed for phosphomimic versions for Na^+ conductance (Figure 2). That AtPIP2;1 can facilitate K^+ transport i*n vivo* adds support to the NSCC hypothesis. The NSCCs observed by Demidchik *et al.,* (2002) had greater K^+ conductance relative to Na^+ conductance (with a selectivity ratio of 1.49:1.00) similar to that observed for K^+ relative to Na^+ conductance for AtPIP2;1 expressed in *X. laevis* oocytes, although the Na^+ substitution for K^+ was not complete as there was 2 mM KCl present in the 'Na100' solution (Figure 2). The regulation of AtPIP2;1 ion transport by cGMP treatments (Figure 1) is also relevant to previous NSCC observations as exogenous application of cGMP was shown to inhibit NSCCs *in planta* (Essah *et al.,* 2003; Maathuis and Sanders, 2001), and intracellular cGMP concentrations have been reported to increase in response to salinity and osmotic stress treatments (Donaldson *et al.,* 2004; Rubio *et al.,* 2003). Interestingly, a recent review hypothesised that Na^+ influx via AtPIP2;1 may be inhibited by cGMP under salt stress (Isayenkov and Maathuis, 2019), which given our results is an idea worth following up *in planta*. Additionally, in the absence of K^+ specific transporters, K^+ uptake in roots was facilitated by an NSCC mechanism sensitive to divalent cations and cNMPs (Caballero *et al.,* 2012; Rubio *et al.,* 2010), that could be contributed to by ion channel aquaporins sensitive to divalent cations (Kourghi *et al.,* 2017) and cNMPs (Figure 1). The observation that AtPIP2;1 facilitates transport of the physiologically important element K^+, and the potential for AtPIP2;1 transport of other monovalent ions such

as NH_4^+, suggests a potential role for PIPs in nutrient acquisition under normal conditions and is also worthy of testing *in planta*.

The central pore, formed in the middle of the four monomeric channels, has been proposed to be the exclusive channel for ion transport through the AtPIP2;1 homotetramer (Kourghi *et al.,* 2018). The phosphorylation state of the CTD is known to be involved in gating of water transport through the monomeric pores, via reinforcing specific steric forms of the cytoplasmic facing loops and protein termini (Frick *et al.,* 2013; Nyblom *et al.,* 2009; Törnroth-Horsefield *et al.,* 2006). Considering the negative correlation between AtPIP2;1 facilitated water and ion transport is linked to the CTD phosphorylation state (Figure 3a), perhaps the CTD is involved in a gating mechanism that differentially regulates AtPIP2;1 function as an ion or water channel. However, whether or not water and ion transport events are mutually exclusive for a single PIP2;1 homotetramer are yet to be determined. Although high ion conductance was more consistently associated with phosphomimic S280 and S283 CTD mutations and high water permeation associated with phosphonull S280 and S283 CTD mutations, this did not necessarily preclude the transport of water and ions respectively (Figure 3b,c and Figure S4). These data indicate that manipulation of phosphorylation at the CTD of AtPIP2;1 might provide a key control point for regulating water and ion net channel selectivity.

Conclusions

This study indicates that differential AtPIP2;1 CTD phosphorylation is a key regulator in the processes controlling water and ion channel transport functions, in addition to localisation trends. Mimicking a phosphorylated state of AtPIP2;1 S280 and S283 sites resulted in increased ion channel function where the Na^+ and K^+ ion conductance reached a magnitude similar to that observed for other plant ion channels expressed in *X. laevis* oocytes, indicating

574 that phosphorylation-dependent ion flux through AtPIP2;1 could be significant *in planta*
575 (McGaughey *et al.,* 2018). Plant aquaporins capable of facilitating ion transport are key
576 candidates for the elusive non-selective cation channels responsible for a large proportion of
577 Na^+ and K^+ flux across the PM (Demidchik *et al.,* 2002; Rubio *et al.,* 2010). Further testing is
578 needed to explore the influence of phosphorylation at S280 and S283 on water and ion
579 transport functions *in planta*, and to resolve whether the observations of AtPIP2;1 potential to
580 switch between ion and water channel modes are translatable. Discovering the mechanisms
581 regulating the switch between ion and water channel functions of some aquaporins, and
582 resolving their relationship with osmotic stress tolerance mechanisms, holds great potential
583 for generating discoveries that contribute to improving plant productivity in dry and saline
584 environments.

585

586 **Acknowledgements**

587 We thank Wendy Sullivan for expert technical assistance, and Apriadi Situmorang for
588 assistance with yeast growth. We thank the Grains Research and Development Corporation
589 (GRDC) for supporting S.M through project number 9174824 and an Australian Bureau of
590 Agricultural and Resource Economics GRDC Science and Innovation Award funding to C.B.
591 This research was supported by the Australian Research Council (ARC) in the form of
592 DP190102725, and Future Fellowship for CB (FT180100476); J.Q. and S.T. were supported
593 through the ARC Centre of Excellence in Plant Energy Biology (CE140100008). MG was
594 funded by the ARC Centre of Excellence for Translational Photosynthesis (CE1401000015).
595 The authors acknowledge the facilities and assistance of Microscopy Australia, Centre for
596 Advanced Microscopy, (CAM), Australian National University.

597

598 The authors have no conflict of interest to declare.

599

600 **Author Contributions**

601 Conceived (CB, ST); planned research (all); cloning for oocyte experiments (JQ); preparation
602 of materials for oocyte experiments (JQ/SM); TEVC (JQ/SM); swelling (SM); oocyte ion
603 content (SM); preparation of yeast materials and cloning (JQ/SM/MG); yeast ion content
604 (JQ); yeast localisation (MG); analysis (all); creation of manuscript draft (SM/JQ/MG);
605 plotting figures and tables for paper (JQ/SM/MG/ST); manuscript revision and editing (all).

606

607 **References**

608

609 **Alberti, S., Gitler, A. D. and Lindquist, S.** (2007). A suite of Gateway® cloning vectors for
610 high-throughput genetic analysis in *Saccharomyces cerevisiae*. *Yeast,* **24**, 913–919.

611 **Anthony, T. L., Brooks, H. L., Boassa, D., Leonov, S., Yanochko, G. M., Regan, J. W.**
612 **and Yool, A. J.** (2000). Cloned human aquaporin-1 Is a cyclic GMP-gated ion channel.
613 *Molecular Pharmacology,* **57**, 576–588.

614 **Banuelos, M. a, Sychrova, H., Bleykasten-Grosshans, C., Souciet, J. and Potier, S.**
615 (1998). The Nha1 antiporter of *Saccharomyces cerevisiae* mediates sodium and
616 potassium efflux. *Microbiology* **144**, 2749–2758.

617 **Bienert, G. P., Moller, A. L. B., Kristiansen, K. A., Schulz, A., Moller, I. M.,**
618 **Schjoerring, J. K. and Jahn, T. P.** (2007). Specific aquaporins facilitate the diffusion
619 of hydrogen peroxide across membranes. *Journal of Biological Chemistry,* **282**, 1183–
620 1192.

621 **Boursiac, Y., Chen, S., Luu, D.-T. T., Sorieul, M., van den Dries, N. and Maurel, C.**

(2005). Early effects of salinity on water transport in *Arabidopsis* roots. Molecular and cellular features of aquaporin expression. *Plant Physiology,* **139**, 790–805.

Boursiac, Y., Boudet, J., Postaire, O., Luu, D.-T. T., Tournaire-Roux, C. and Maurel, C. (2008). Stimulus-induced downregulation of root water transport involves reactive oxygen species-activated cell signalling and plasma membrane intrinsic protein internalization. *The Plant Journal,* **56**, 207–218.

Byrt, C. S., Zhao, M., Kourghi, M., Bose, J., Henderson, S. W., Qiu, J., Gilliham, M., Schultz, C., Schwarz, M., Ramesh, S. A., et al. (2017). Non-selective cation channel activity of aquaporin AtPIP2;1 regulated by $Ca^{2+}$and pH. *Plant, Cell and Environment,* **40**, 802–815.

Caballero, F., Botella, M. A., Rubio, L., Fernández, J. A., Martínez, V., Rubio, F., Fernandez, J. A., Martinez, V. and Rubio, F. (2012). A Ca^{2+}-sensitive system mediates low-affinity K^+ uptake in the absence of AKT1 in arabidopsis plants. *Plant Cell Physiology,* **53**, 2047–2059.

Campbell, E. M., Birdsell, D. N. and Yool, A. J. (2012). The activity of human aquaporin 1 as a cGMP-gated cation channel is regulated by tyrosine phosphorylation in the carboxyl-terminal domain. *Molecular Pharmacology,* **81**, 97–105.

Chaumont, F. and Tyerman, S. D. (2014). Aquaporins: Highly regulated channels controlling plant water relations. *Plant Physiology,* **164**, 1600–1618.

Chaumont, F. and Tyerman, S. D. (2017). *Plant Aquaporins*. (ed. Francois Chaumont, S. D. T.) Springer.

Conti, M., Hsieh, M., Musa Zamah, A. and Oh, J. S. (2012). Novel signaling mechanisms in the ovary during oocyte maturation and ovulation. *Molecular and Cellular*

Endocrinology, **356**, 65–73.

De Ieso, M. L. and Yool, A. J. (2018). Mechanisms of aquaporin-facilitated cancer invasion and metastasis. *Frontiers in Chemistry,* **6**, 135.

Demidchik, V., Davenport, R. J. and Tester, M. (2002). Nonselective cation channels in plants. *Annual Review of Plant Biology,* **53**, 67–107.

di Pietro, M., Vialaret, J., Li, G.-W., Hem, S., Prado, K., Rossignol, M., Maurel, C. and Santoni, V. (2013). Coordinated post-translational responses of aquaporins to abiotic and nutritional stimuli in Arabidopsis roots. *Molecular and Cellular Proteomics,* **12**, 3886–3897.

Donaldson, L., Ludidi, N., Knight, M. R., Gehring, C. and Denby, K. (2004). Salt and osmotic stress cause rapid increases in *Arabidopsis thaliana* cGMP levels. *FEBS Letters,* **569**, 317–320.

Dynowski, M., Schaaf, G., Loque, D., Moran, O. and Ludewig, U. (2008a). Plant plasma membrane water channels conduct the signalling molecule H_2O_2. *Biochemical Journal,* **414**, 53–61.

Dynowski, M., Mayer, M., Moran, O. and Ludewig, U. (2008b). Molecular determinants of ammonia and urea conductance in plant aquaporin homologs. *FEBS Letters,* **582**, 2458–2462.

Essah, P. A., Davenport, R. and Tester, M. (2003). Sodium influx and accumulation in Arabidopsis. *Plant Physiology,* **133**, 307–318.

Eto, K., Noda, Y., Horikawa, S., Uchida, S. and Sasaki, S. (2010). Phosphorylation of aquaporin-2 regulates its water permeability. *Journal of Biological Chemistry,* **285**, 40777–40784.

668 **Fenton, R. A., Moeller, H. B., Hoffert, J. D., Yu, M.-J., Nielsen, S. and Knepper, M. A.**
669 (2008). Acute regulation of aquaporin-2 phosphorylation at Ser-264 by vasopressin.
670 *Proceedings of the National Academy of Sciences,* **105**, 3134–3139.

671 **Fischer, G., Kosinska-Eriksson, U., Aponte-Santamaría, C., Palmgren, M., Geijer, C.,**
672 **Hedfalk, K., Hohmann, S., De Groot, B. L., Neutze, R. and Lindkvist-Petersson, K.**
673 (2009). Crystal structure of a yeast aquaporin at 1.15 Å reveals a novel gating
674 mechanism. *PLoS Biology* **7**, 6.

675 **Francis, S. H. and Corbin, J. D.** (1999). Cyclic nucleotide-dependent protein kinases :
676 intracellular receptors for cAMP and cGMP action. *Critical Reviews in Clinical*
677 *Laboratory Services,* **34**, 275–328.

678 **Frick, A., Järvå, M., Törnroth-Horsefield, S., Jarva, M., Tornroth-Horsefield, S., Järvå,**
679 **M. and Törnroth-Horsefield, S.** (2013). Structural basis for pH gating of plant
680 aquaporins. *FEBS Letters,* **587**, 989–993.

681 **Gambetta, G. A., Knipfer, T., Fricke, W. and McElrone, A. J.** (2017). Aquaporins and
682 root water uptake. In *Plant Aquaporins*, pp. 133–153. Springer.

683 **Gerbeau, P., Guclu, J., Ripoche, P. and Maurel, C.** (1999). Aquaporin Nt-TIPα can
684 account for the high permeability of tobacco cell vacuolar membrane to small neutral
685 solutes. *The Plant Journal,* **18**, 577–587.

686 **Glass, D. B. and Krebs, E. G.** (1980). Protein phosphorylation catalyzed by cyclic AMP-
687 dependent and cyclic GMP-dependent protein kinases. *Annual Review of Pharmocology*
688 *and Toxicology,* **20**, 363-388.

689 **Grondin, A., Rodrigues, O., Verdoucq, L., Merlot, S., Leonhardt, N. and Maurel, C.**
690 (2015). Aquaporins contribute to ABA-triggered stomatal closure through OST1-

691 mediated phosphorylation. *The Plant Cell* **27**, 1945–1954.

692 **Groszmann, M., Osborn, H. L. and Evans, J. R.** (2017). Carbon dioxide and water
693 transport through plant aquaporins. *Plant, Cell and Environment,* **40**, 938–961.

694 **Guenther, J. F., Chanmanivone, N., Galetovic, M. P., Wallace, I. S., Cobb, J. A. and**
695 **Roberts, D. M.** (2003). Phosphorylation of soybean nodulin 26 on serine 262 enhances
696 water permeability and is regulated developmentally and by osmotic signals. *The Plant*
697 *Cell* **15**, 981–991.

698 **Gunnarson, E., Axehult, G., Baturina, G., Zelenin, S., Zelenina, M. and Aperia, A.**
699 (2005). Lead induces increased water permeability in astrocytes expressing aquaporin 4.
700 *Neuroscience* **136**, 105–114.

701 **Han, Z. and Patil, R. V** (2000). Protein kinase A-dependent phosphorylation of aquaporin-1.
702 *Biochemical and Biophysical Research Communications,* **273**, 328–332.

703 **Hoffert, J. D., Pisitkun, T., Wang, G., Shen, R.-F. and Knepper, M. A.** (2006).
704 Quantitative phosphoproteomics of vasopressin-sensitive renal cells: Regulation of
705 aquaporin-2 phosphorylation at two sites. *Proceedings of the National Academy of*
706 *Science,* **103**, 7159–7164.

707 **Hoffert, J. D., Fenton, R. A., Moeller, H. B., Simons, B., Tchapyjnikov, D., McDill, B.**
708 **W., Yu, M. J., Pisitkun, T., Chen, F. and Knepper, M. A.** (2008). Vasopressin-
709 stimulated increase in phosphorylation at Ser269 potentiates plasma membrane retention
710 of aquaporin-2. *Journal of Biological Chemistry.* **283**, 24617–24627.

711 **Hooijmaijers, C., Rhee, J. Y., Kwak, K. J., Chung, G. C., Horie, T., Katsuhara, M. and**
712 **Kang, H.** (2012). Hydrogen peroxide permeability of plasma membrane aquaporins of
713 *Arabidopsis thaliana*. *Journal of Plant Research,* **125**, 147–153.

Horie, T., Kaneko, T., Sugimoto, G., Sasano, S., Panda, S. K., Shibasaka, M. and Katsuhara, M. (2011). Mechanisms of water transport mediated by PIP aquaporins and their regulation via phosphorylation events under salinity stress in Barley roots. *Plant Cell Physiology,* **52**, 663–675.

Isayenkov, S. V and Maathuis, F. J. M. (2019). Plant salinity stress: Many unanswered questions remain. *Fronteirs in Plant Science.* **10**, 80.

Jang, H. Y., Rhee, J., Carlson, J. E. and Ahn, S. J. (2014). The Camelina aquaporin CsPIP2;1 is regulated by phosphorylation at Ser273, but not at Ser277, of the C-terminus and is involved in salt- and drought-stress responses. *Journal of Plant Physiology,* **171**, 1401–1412.

Johansson, I., Karlsson, M., Shukla, V. K., Chrispeels, M. J., Larsson, C. and Kjellbom, P. (1998). Water transport activity of the plasma membrane aquaporin PM28A is regulated by phosphorylation. *The Plant Cell* **10**, 451–459.

Kourghi, M., Pei, J. V, De Ieso, M. L., Flynn, G. and Yool, A. J. (2015). Bumetanide derivatives AqB007 and AqB011 selectively block the Aquaporin-1 ion channel conductance and slow cancer cell migration. *Molecular Pharmacology,* **89**, 133–140.

Kourghi, M., Nourmohammadi, S., Pei, J., Qiu, J., McGaughey, S., Tyerman, S., Byrt, C. and Yool, A. (2017). Divalent cations regulate the ion conductance properties of diverse classes of aquaporins. *International Journal of Molecular Sciences,* **18**, 2323.

Kourghi, M., Pei, J. V, De Ieso, M. L., Nourmohammadi, S., Chow, P. H. and Yool, A. J. (2018). Fundamental structural and functional properties of Aquaporin ion channels found across the kingdoms of life. *Clinical and Experimental Pharmacology and Physiology,* **45**, 401–409.

Kuwahara, M., Fushimi, K., Terada, Y., Liqun, B., Marumo, F. and Sasaki, S. (1995). cAMP-dependent phosphorylation stimulates water permeability of aquaporin-collecting duct water channel protein expressed in *Xenopus* oocytes. *Journal of Biological Chemistry,* **270**, 10384–10387.

Lee, J. W., Zhang, Y., Weaver, C. D., Shomer, N. H., Louis, C. F. and Roberts, D. M. (1995). Phosphorylation of Nodulin 26 on Serine 262 affects its voltage-sensitive channel activity in planar lipid bilayers. *Journal of Biological Chemistry,* **270**, 27051–27057.

Li, R. Y., Ago, Y., Liu, W. J., Mitani, N., Feldmann, J., McGrath, S. P., Ma, J. F. and Zhao, F. J. (2009). The rice aquaporin Lsi1 mediates uptake of methylated arsenic species. *Plant Physiology,* **150**, 2071–2080.

Li, X., Wang, X., Yang, Y., Li, R., He, Q., Fang, X., Luu, D.-T., Maurel, C. and Lin, J. (2011). Single-molecule analysis of PIP2;1 dynamics and partitioning reveals multiple modes of *Arabidopsis* plasma membrane aquaporin regulation. *The Plant Cell,* **23**, 3780–3797.

Liu, S., Fukumoto, T., Gena, P., Feng, P., Sun, Q., Li, Q., Matsumoto, T., Kaneko, T., Zhang, H., Zhang, Y., et al. (2020). Ectopic expression of a rice plasma membrane intrinsic protein (OsPIP1;3) promotes plant growth and water uptake. *Plant Journal,* **102**, 779–796.

Loqué, D., Ludewig, U., Yuan, L. and von Wirén, N. (2005). Tonoplast intrinsic proteins AtTIP2;1 and AtTIP2;3 facilitate NH_3 transport into the vacuole. *Plant Physiology,* **137**, 671–680.

Lu, H. J., Matsuzaki, T., Bouley, R., Hasler, U., Qin, Q. H. and Brown, D. (2008). The phosphorylation state of serine 256 is dominant over that of serine 261 in the regulation

761 of AQP2 trafficking in renal epithelial cells. *American Journal of Physiology - Renal*
762 *Physiology,* **295**, 290–294.

763 **Luu, D. T., Martiniãre, A., Sorieul, M., Runions, J., Maurel, C., Martiniere, A., Sorieul,**
764 **M., Runions, J. and Maurel, C.** (2012). Fluorescence recovery after photobleaching
765 reveals high cycling dynamics of plasma membrane aquaporins in Arabidopsis roots
766 under salt stress. *Plant Journal,* **69**, 894–905.

767 **Ma, J. F., Tamai, K., Yamaji, N., Mitani, N., Konishi, S., Katsuhara, M., Ishiguro, M.,**
768 **Murata, Y. and Yano, M.** (2006). A silicon transporter in rice. *Nature* **440**, 688–691.

769 **Maathuis, F. J. and Sanders, D.** (2001). Sodium uptake in *Arabidopsis* roots is regulated by
770 cyclic nucleotides. *Plant Physiology,* **127**, 1617–25.

771 **Maurel, C., Kado, R. T., Guern, J. and Chrispeels, M. J.** (1995). Phosphorylation
772 regulates the water channel activity of the seed-specific aquaporin α-Tip. *The EMBO*
773 *Journal,* **14**, 3028–3035.

774 **Maurel, C., Boursiac, Y., Luu, D. T. D.-T. T., Santoni, V., Shahzad, Z. and Verdoucq, L.**
775 (2015). Aquaporins in plants. *Physiological Reviews,* **95**, 1321–1358.

776 **McGaughey, S. A., Qiu, J., Tyerman, S. D. and Byrt, C. S.** (2018). Regulating root
777 aquaporin function in response to changes in salinity. *Annual Plant Reviews Online* **1**,
778 1–36.

779 **Metzger, M. B., Maurer, M. J., Dancy, B. M. and Michaelis, S.** (2008). Degradation of a
780 cytosolic protein requires endoplasmic reticulum-associated degradation machinery.
781 *Journal of Biological Chemistry,* **283**, 32302–32316.

782 **Moeller, H. B., Praetorius, J., Rutzler, M. R. and Fenton, R. A.** (2010). Phosphorylation
783 of aquaporin-2 regulates its endocytosis and protein-protein interactions. *Proceedings of*

784 *the National Academy of Science.* **107**, 424–429.

785 **Munns, R., Day, D. A., Fricke, W., Watt, M., Arsova, B., Barkla, B. J., Bose, J., Byrt, C.**
786 **S., Chen, Z., Foster, K. J., et al.** (2020). Energy costs of salt tolerance in crop plants.
787 *New Phytologist,* **255,** 1072-1090

788 **Nyblom, M., Frick, A., Wang, Y., Ekvall, M., Hallgren, K., Hedfalk, K., Neutze, R.,**
789 **Tajkhorshid, E. and Törnroth-Horsefield, S.** (2009). Structural and functional
790 analysis of SoPIP2;1 mutants adds insight into plant aquaporin gating. *Journal of*
791 *Molecular Biology,* **387**, 653–668.

792 **Otto, B., Uehlein, N., Sdorra, S., Fischer, M., Ayaz, M., Belastegui-Macadam, X.,**
793 **Heckwolf, M., Lachnit, M., Pede, N., Priem, N., et al.** (2010). Aquaporin tetramer
794 composition modifies the function of Tobacco aquaporins. *Journal of Biological*
795 *Chemistry,* **285**, 31253–31260.

796 **Prado, K. and Maurel, C.** (2013). Regulation of leaf hydraulics: From molecular to whole
797 plant levels. *Frontiers in Plant Science,* **4**, 1–14.

798 **Prado, K., Cotelle, V., Li, G., Bellati, J., Tang, N., Tournaire-Roux, C., Martiniere, A.,**
799 **Santoni, V., Maurel, C., Martiniere, A., et al.** (2019). Oscillating aquaporin
800 phosphorylations and 14-3-3 proteins mediate circadian regulation of leaf hydraulics.
801 *The Plant Cell* **4**, tpc.00804.2018.

802 **Prak, S., Hem, S., Boudet, J., Viennois, G., Sommerer, N., Rossignol, M., Maurel, C.**
803 **and Santoni, V.** (2008). Multiple phosphorylations in the C-terminal tail of plant
804 plasma membrane aquaporins. *Molecular and Cellular Proteomics* **7**, 1019–1030.

805 **Qing, D., Yang, Z., Li, M., Wong, W. S., Guo, G., Liu, S., Guo, H. and Li, N.** (2016).
806 Quantitative and functional phosphoproteomic analysis reveals that ethylene regulates

water transport via the C-Terminal phosphorylation of aquaporin PIP2;1 in *Arabidopsis*. *Molecular Plant,* **9**, 158–174.

Qiu, J., Henderson, S. W., Tester, M., Roy, S. J. and Gilliham, M. (2016). SLAH1, a homologue of the slow type anion channel SLAC1, modulates shoot Cl^- accumulation and salt tolerance in *Arabidopsis thaliana*. *Journal of Experimental Botany,* **67**, 4495–4505.

Roberts, S. K. and Tester, M. (1997). A patch clamp study of Na^+ transport in maize roots. *Journal of Experimental Botany,* **48**, 431–440.

Rodrigues, O., Reshetnyak, G., Grondin, A., Saijo, Y., Leonhardt, N., Maurel, C. and Verdoucq, L. (2017). Aquaporins facilitate hydrogen peroxide entry into guard cells to mediate ABA- and pathogen-triggered stomatal closure. *Proceedings of the National Academy of Science,* **114**, 9200–9205.

Rubio, F., Flores, P., Navarro, J. M. and Martínez, V. (2003). Effects of Ca^{2+}, $K^+$and cGMP on Na^+ uptake in pepper plants. *Plant Science,* **165**, 1043–1049.

Rubio, F., Alemán, F., Nieves-Cordones, M. and Martínez, V. (2010). Studies on Arabidopsis athak5, atakt1 double mutants disclose the range of concentrations at which AtHAK5, AtAKT1 and unknown systems mediate K^+ uptake. *Physiologia Plantarum,* **139**, 220–228.

Takano, J., Wada, M., Ludewig, U., Schaaf, G., Von Wirén, N. and Fujiwara, T. (2006). The Arabidopsis major intrinsic protein NIP5;1 is essential for efficient boron uptake and plant development under boron limitation. *The Plant Cell* **18**, 1498–1509.

Tanghe, A., Van Dijck, P., Dumortier, F., Teunissen, A., Hohmann, S. and Thevelein, J. M. (2002). Aquaporin expression correlates with freeze tolerance in baker's yeast, and

overexpression improves freeze tolerance in industrial strains. *Applied and Environmental Microbiology,* **68**, 5981–5989.

Törnroth-Horsefield, S., Wang, Y., Hedfalk, K., Johanson, U., Karlsson, M., Tajkhorshid, E., Neutze, R. and Kjellbom, P. (2006). Structural mechanism of plant aquaporin gating. *Nature* **439**, 688–694.

Tournaire-Roux, C., Sutka, M., Javot, H. H., Gout, E. E., Gerbeau, P., Luu, D.-T. T., Bligny, R. and Maurel, C. (2002). Cytosolic pH regulates root water transport during anoxic stress through gating of aquaporins. *Nature* **425**, 187–194.

Ueda, M., Tsutsumi, N. and Fujimoto, M. (2016). Salt stress induces internalization of plasma membrane aquaporin into the vacuole in *Arabidopsis thaliana*. *Biochemical and Biophysical Research Communications,* **474**, 742–746.

Uehlein, N., Lovisolo, C., Siefritz, F. and Kaldenhoff, R. (2003). The tobacco aquaporin NtAQP1 is a membrane CO_2 pore with physiological functions. *Nature* **425**, 734–737.

Uehlein, N., Otto, B., Eilingsfeld, A., Itel, F., Meier, W. and Kaldenhoff, R. (2012). Gas-tight triblock-copolymer membranes are converted to CO_2 permeable by insertion of plant aquaporins. *Scientific Reports,* **2**, 538.

Van Balkom, B. W. M., Savelkoul, P. J. M., Markovich, D., Hofman, E., Nielsen, S., Van Der Sluijs, P. and Deen, P. M. T. (2002). The role of putative phosphorylation sites in the targeting and shuttling of the aquaporin-2 water channel. *Journal of Biological Chemistry,* **277**, 41473–41479.

Van Wilder, V., Miecielica, U., Degand, H., Derua, R., Waelkens, E. and Chaumont, F. (2008). Maize plasma membrane aquaporins belonging to the PIP1 and PIP2 subgroups are in vivo phosphorylated. *Plant Cell Physiology,* **49**, 1364–1377.

Weaver, C. D., Shomer, N. H., Louis, C. F. and Roberts, D. M. (1994). Nodulin 26, a nodule-specific symbiosome membrane protein from Soybean, is an ion channel. *Journal of Biological Chemistry,* **269**, 17858–17862.

Yaneff, A., Sigaut, L., Gómez, N., Aliaga Fandiño, C., Alleva, K., Pietrasanta, L. I. and Amodeo, G. (2016). Loop B serine of a plasma membrane aquaporin type PIP2 but not PIP1 plays a key role in pH sensing. *Biochimica et Biophysica Acta – Biomembranes,* **1858**, 2778–2787.

Yanochko, G. M. and Yool, A. J. (2002). Regulated cationic channel function in *Xenopus* oocytes expressing *Drosophila* Big Brain. *The Journal of Neuroscience.* **22**, 2530–2540.

Yool, A. J., Stamer, W. D. and Regan, J. W. (1996). Forskolin stimulation of water and cation permeability in aquaporin1 water channels. *Science,* **273**, 1216–1218.

Zelenina, M., Zelenin, S., Bondar, A. A., Brismar, H. and Aperia, A. (2002). Water permeability of aquaporin-4 is decreased by protein kinase C and dopamine. *American Journal of Renal Physiology,* **283**, F309-F318.

Zhang, W., Zitron, E., Hö, M., Kihm, L., Morath, C., Scherer, D., Hegge, S., Thomas, D., Schmitt, C. P., Zeier, M., et al. (2007). Aquaporin-1 channel function is positively regulated by protein kinase C. *Journal of Biological Chemistry,* **282**, 20933–20940.

Zwiazek, J. J., Xu, H., Tan, X., Navarro-Ródenas, A., Morte, A., Benga, G., Popescu, O., Pop, V. I., Holmes, R., Agre, P., et al. (2017). Significance of oxygen transport through aquaporins. *Scientific Reports,* **7**, 40411.

874 **Figure 1: Exogenous application of membrane permeable cAMP and cGMP analogues**
875 **as kinase stimulators and the kinase inhibitor H7 influence ionic conductance of**
876 ***AtPIP2;1*** **injected oocytes.** Oocytes were either untreated or were pre-treated in Low Na^+
877 Ringers solution that contained 1 mM 8-Br-cAMP (cAMP), 1 mM 8-Br-cGMP (cGMP) or 10
878 µM H7 dihydrochloride (H7) or H7 followed by cAMP/cGMP. TEVC was performed in a
879 'Na50' solution. The ionic conductance of treated water injected and *AtPIP2;1* cRNA
880 injected oocytes were normalised to untreated water injected and *AtPIP2;1* cRNA injected
881 oocytes respectively. **(a)** Relative ionic conductance of control oocytes. **(b)** Relative ionic
882 conductance of *AtPIP2;1* injected oocytes. Data was compiled from at least two independent
883 oocytes batches with the exception of the H7 + cNMP treatment where data from one batch
884 of oocytes is represented. Data is represented as mean relative conductance ± SEM where
885 each point represents a single oocyte. Significant differences ($P < 0.001$) are indicated by
886 different letters using one-way ANOVA, Fisher's post test, or by an * (un-paired t-test).

Figure 2: Phosphorylation mimic of AtPIP2;1 S280 and S283 residues influence AtPIP2;1 facilitated cation transport. Oocytes were injected with 46 nL water (Control) or with 46 nL water containing 23 ng *AtPIP2;1* WT (WT) or S280A, S280D, S283A, S283D, A/A, D/A, A/D or D/D cRNA. Representative superimposed currents as a function of time of **(a)** AtPIP2;1 single phosphorylation mutants in 'Na100' (Na^+; note that there was 2 mM KCl in this solution) and 'K100' (K^+), and **(b)** AtPIP2;1 double phosphorylation mutants in 'Na100' (Na^+). Currents were recorded starting from -40 mV holding potential for 0.5 s and ranging from 40 mV to –120 mV with 20 mV decrements for 0.5 s before following a –40 mV pulse for another 0.5 s. Ionic conductance of oocytes expressing **(c)** AtPIP2;1 single phosphorylation mutants in 'Na100' (Na^+) and 'K100' (K^+), and **(d)** AtPIP2;1 double phosphorylation mutants in 'Na100' (Na^+). Ionic conductance was calculated by taking the slope of a regression of the linear region across the reversal potential (–60 mV to +40 mV). **(e)** Na^+ content of oocytes incubated in 'Na100' for 24 h. Data in (c-e) is compiled from three independent oocyte batches and is shown as mean ± SEM where each data point represents an individual oocyte. Significant differences ($P<0.05$) are indicated by different letters (one-way ANOVA, Fisher's post-test), or by an * (un-paired t-test). From this data for WT and the different mutants the following was calculated: WT, g_K/g_{Na}= 1.54 (1.28); S280D, g_K/g_{Na} = 1.44 (1.20); S280A, g_K/g_{Na} = 0.9 (0.82); S283D, g_K/g_{Na} = 1.33 (1.24); and S283A, g_K/g_{Na} = 0.333 (0.14) where g_K/g_{Na} is the mean of g_K divided by the mean of g_{Na} and values within brackets is the mean of g_K relative to H_2O divided by the mean of g_{Na} relative to H_2O.

907 **Figure 3. Phosphorylation mimics of AtPIP2;1 S280 and S283 residues influences its**
908 **osmotic water permeability and the relationship between osmotic water permeability**
909 **and ionic conductance.** Osmotic water permeability (P_{os}) and ionic conductance of water
910 injected (n= 13) and AtPIP2;1 Wild-type (n=37), S280D (n=20) , S280A (n= 13), S283D (n=
911 19), S283A (n= 17), A/A(n= 25), D/A (n= 16), A/D (n= 27) or AtPIP2;1 D/D (n= 30) cRNA
912 injected oocytes was determined via the swelling assay and TEVC, respectively. **(a)** Ionic
913 conductance collected from multiple batches were allocated into 10 μS bins and the mean ±
914 SEM of each binned group and corresponding P_{os} is plotted. Individual conductance was
915 plotted against the corresponding P_{os} for each oocyte (data shown in Figure S3). A single
916 exponential decay best fit the combined data ($P< 0.005$). The red and blue dashed lines
917 indicate the mean ionic conductance and P_{os} of water injected (control) oocytes. **(b)**
918 Frequency histogram of P_{os} for each of the phosphomimics in decreasing order of the mean
919 P_{os} from left to right. The blue dashed line in each histogram indicated the mean of Pos in
920 water injected (control) oocytes. **(c)** Frequency histogram of ionic conductance for each of
921 the phosphomimics in increasing order of the mean from left to right. The red dashed line in
922 each histogram indicated the mean of ionic conductance in water injected (control) oocytes.
923 **(d)** Comparison of the order of decreasing P_{os} and increasing ionic conductance. Genotypes
924 marked by shaded boxes follow the same relative order for the change in mean P_{os} and ionic
925 conductance.

926 **Figure 4: Intracellular Na^+ accumulation varied in yeast expressing AtPIP2;1 CTD**
927 **phosphorylation mimic mutants.** Empty vector, AtPIP2;7, AtPIP2;1WT and all versions of
928 CTD of AtPIP2;1 mutants were each expressed in the B31 yeast mutant strain. After
929 suspension in NaCl uptake buffer (70 mM NaCl, 10 mM MES, 10 mM EGTA, pH5.6) for 40
930 min, intracellular Na^+ contents were measured. Data are compiled from three independent
931 experimental batches each comprised of three independent replicate cultures, and is
932 represented as mean ± SEM. Significant differences (P <0.05) are indicated by different
933 letters (one-way ANOVA, Fisher's post-test). N= Empty (10), AtPIP2;7 (7), AtPIP2;1 WT
934 (10), S280A (7), S280D (7), S283A (7), S283D (10), A/D (7), D/A (7), AtPIP2;1 A/A (7) and
935 D/D (7).

Figure 5: Subcellular localisation of AtPIP2;1 wild-type and S280/S283 phospho-mutants in yeast. **(a)** GFP control with diffuse cytosolic localised signal. **(b)** SEC63::RFP endoplasmic reticulum marker. The yeast ER network consists of the prominent nuclear envelope ER domain (nER) and a peripheral or cortical ER domain (cER). The cER lies just beneath the plasma membrane but is not continuous around the perimeter with gaps distinguishing it from plasma membrane localisation (solid triangle). Cytoplasmic tubules link the two ER domains (*). **(c)** Wild-type AtPIP2;1::eGFP localises to a distinct continuous ring of expression around the cell perimeter coinciding with the plasma membrane (PM). GFP signal is also weakly present in the tonoplast of the vacuole (V). In this example, no expression is detected in the nER. **(d-e)** The single phospho-mimetic S280D mutant commonly shows a continuous ring of PM localisation along with a substantially stronger GFP signal co-localised with the ER marker in both the peripheral (open arrow heads) and internal ER networks (nER). **(f)** The single phospho-mimetic S283D mutant shows a distinct localisation around the PM with little to no ER co-localisation. Weak GFP signal is occasionally observed in the periphery of the vacuoles (V). **(g-h)** The localisation of the double phosphorylated mimetic D/D mutant occurs almost exclusively in the PM with comparably weak signal detectable in the tonoplast of the vacuole (V) and little to no signal in the ER. **(i)** The double A/D mutant localises to the PM. Approximately half the yeast cells examined also exhibit strong co-localisation to the ER. **(j)** The frequency of yeast cells with GFP signal detected in the PM only versus co-localisation in both the PM and ER. Asterisks (*) denote statistically significant difference (Fisher's exact test $p \leq 0.05$). N = WtAtPIP2;1(53), S280A(57), S283S(161), S283A(32), S283D(94), A/A(117), D/A(64), A/D(139) , D/D(83).

Summary Statement

Salt-stress associated changes in the phosphorylation state of Arabidopsis dual water-ion permeable aquaporin AtPIP2;1 influence its channel function. Testing in a heterologous system revealed a phosphorylation-mimic dependent negative relationship between AtPIP2;1 water and ion channel function.

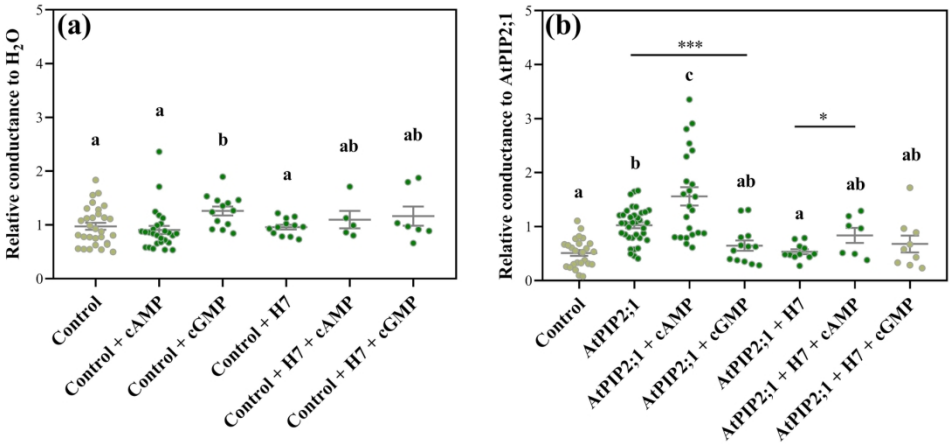

Figure 1: Exogenous application of membrane permeable cAMP and cGMP analogues as kinase stimulators and the kinase inhibitor H7 influence ionic conductance of AtPIP2;1 injected oocytes. Oocytes were either untreated or were pre-treated in Low Na^+ Ringers solution that contained 1 mM 8-Br-cAMP (cAMP), 1 mM 8-Br-cGMP (cGMP) or 10 µM H7 dihydrochloride (H7) or H7 followed by cAMP/cGMP. TEVC was performed in a 'Na50' solution. The ionic conductance of treated water injected and AtPIP2;1 cRNA injected oocytes were normalised to untreated water injected and AtPIP2;1 cRNA injected oocytes respectively. **(a)** Relative ionic conductance of control oocytes. **(b)** Relative ionic conductance of AtPIP2;1 injected oocytes. Data was compiled from at least two independent oocytes batches with the exception of the H7 + cNMP treatment where data from one batch of oocytes is represented. Data is represented as mean relative conductance ± SEM where each point represents a single oocyte. Significant differences ($P < 0.001$) are indicated by different letters using one-way ANOVA, Fisher's post test, or by an * (un-paired t-test).

169x85mm (300 x 300 DPI)

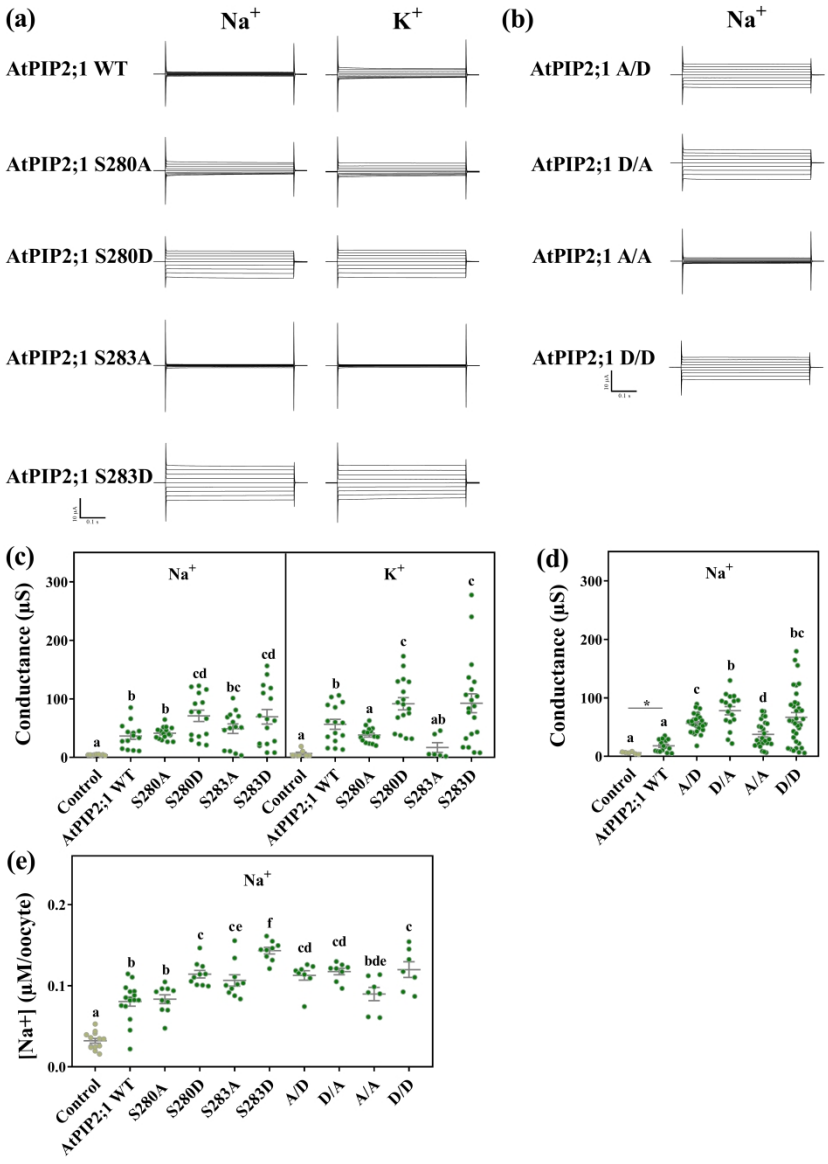

Figure 2: Phosphorylation mimic of AtPIP2;1 S280 and S283 residues influence AtPIP2;1 facilitated cation transport. Oocytes were injected with 46 nL water (Control) or with 46 nL water containing 23 ng AtPIP2;1 WT (WT) or S280A, S280D, S283A, S283D, A/A, D/A, A/D or D/D cRNA. Representative superimposed currents as a function of time of **(a)** AtPIP2;1 single phosphorylation mutants in 'Na100' (Na^+; note that there was 2 mM KCl in this solution) and 'K100' (K^+), and **(b)** AtPIP2;1 double phosphorylation mutants in 'Na100' (Na^+). Currents were recorded starting from -40 mV holding potential for 0.5 s and ranging from 40 mV to –120 mV with 20 mV decrements for 0.5 s before following a –40 mV pulse for another 0.5 s. Ionic conductance of oocytes expressing **(c)** AtPIP2;1 single phosphorylation mutants in 'Na100' (Na^+) and 'K100' (K^+), and **(d)** AtPIP2;1 double phosphorylation mutants in 'Na100' (Na^+). Ionic conductance was calculated by taking the slope of a regression of the linear region across the reversal potential (–60 mV to +40 mV). **(e)** Na^+ content of oocytes incubated in 'Na100' for 24 h. Data in (c-e) is compiled from three independent oocyte batches and is shown as mean ± SEM where each data

point represents an individual oocyte. Significant differences ($P<0.05$) are indicated by different letters (one-way ANOVA, Fisher's post-test), or by an * (un-paired t-test). From this data for WT and the different mutants the following was calculated: WT, g_K/g_{Na}= 1.54 (1.28); S280D, g_K/g_{Na} = 1.44 (1.20); S280A, g_K/g_{Na} = 0.9 (0.82); S283D, g_K/g_{Na} = 1.33 (1.24); and S283A, g_K/g_{Na} = 0.333 (0.14) where g_K/g_{Na} is the mean of g_K divided by the mean of g_{Na} and values within brackets is the mean of g_K relative to H_2O divided by the mean of g_{Na} relative to H_2O.

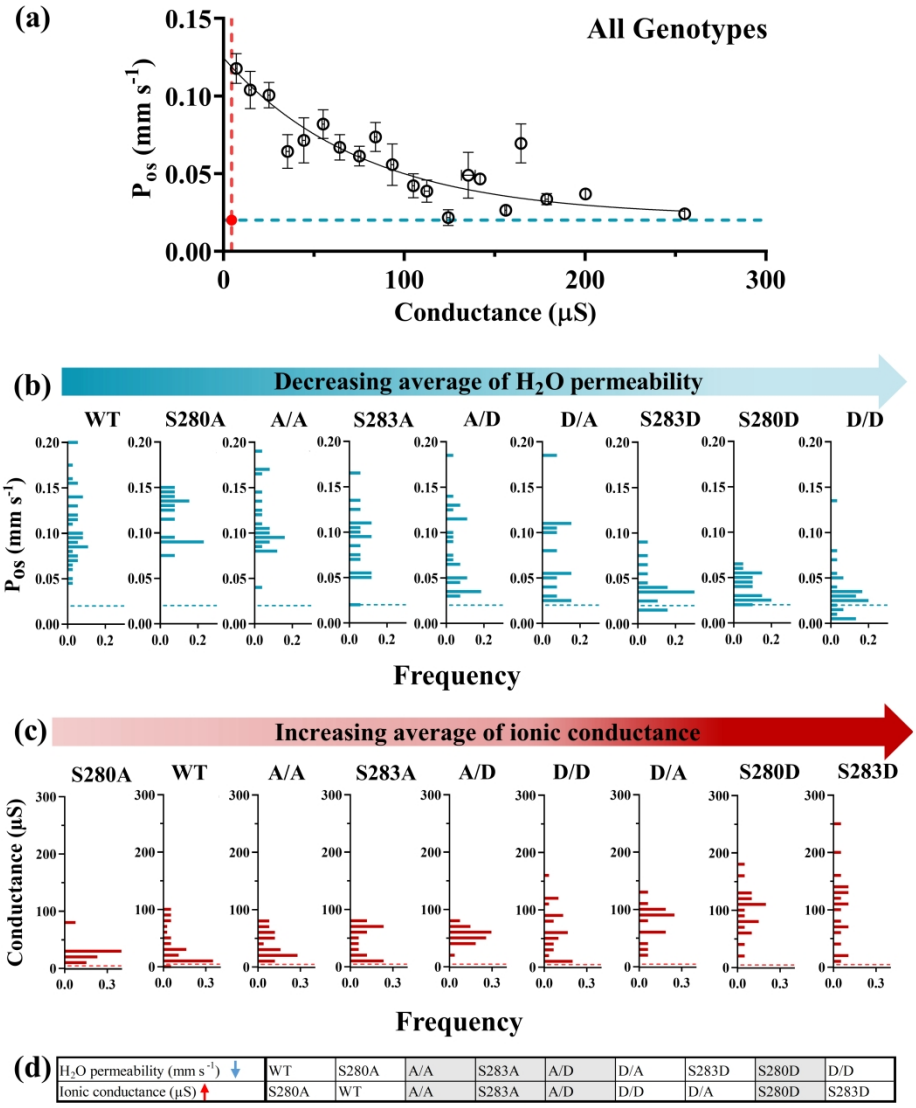

Figure 3. Phosphorylation mimics of AtPIP2;1 S280 and S283 residues influences its osmotic water permeability and the relationship between osmotic water permeability and ionic conductance. Osmotic water permeability (P_{os}) and ionic conductance of water injected (n= 13) and AtPIP2;1 Wild-type (n=37), S280D (n=20) , S280A (n= 13), S283D (n= 19), S283A (n= 17), A/A(n= 25), D/A (n= 16), A/D (n= 27) or AtPIP2;1 D/D (n= 30) cRNA injected oocytes was determined via the swelling assay and TEVC, respectively. **(a)** Ionic conductance collected from multiple batches were allocated into 10 μS bins and the mean ± SEM of each binned group and corresponding P_{os} is plotted. Individual conductance was plotted against the corresponding P_{os} for each oocyte (data shown in Figure S3). A single exponential decay best fit the combined data (P< 0.005). The red and blue dashed lines indicate the mean ionic conductance and P_{os} of water injected (control) oocytes. **(b)** Frequency histogram of P_{os} for each of the phosphomimics in decreasing order of the mean P_{os} from left to right. The blue dashed line in each histogram indicated the mean of P_{os} in water injected (control) oocytes. **(c)** Frequency histogram of ionic conductance for each of the phosphomimics in increasing order of the mean from left to right. The red

dashed line in each histogram indicated the mean of ionic conductance in water injected (control) oocytes. **(d)** Comparison of the order of decreasing P_{os} and increasing ionic conductance. Genotypes marked by shaded boxes follow the same relative order for the change in mean P_{os} and ionic conductance.

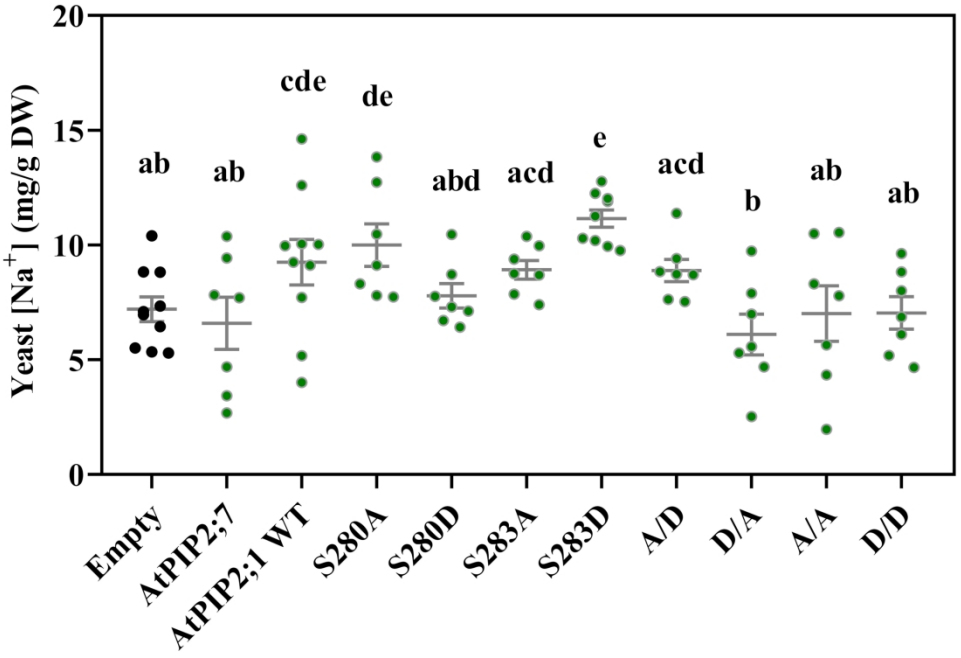

Figure 4: Intracellular Na^+ accumulation varied in yeast expressing AtPIP2;1 CTD phosphorylation mimic mutants. Empty vector, AtPIP2;7, AtPIP2;1WT and all versions of CTD of AtPIP2;1 mutants were each expressed in the B31 yeast mutant strain. After suspension in NaCl uptake buffer (70 mM NaCl, 10 mM MES, 10 mM EGTA, pH5.6) for 40 min, intracellular Na^+ contents were measured. Data are compiled from three independent experimental batches each comprised of three independent replicate cultures, and is represented as mean ± SEM. Significant differences ($P < 0.05$) are indicated by different letters (one-way ANOVA, Fisher's post-test). N= Empty (10), AtPIP2;7 (7), AtPIP2;1 WT (10), S280A (7), S280D (7), S283A (7), S283D (10), A/D (7), D/A (7), AtPIP2;1 A/A (7) and D/D (7).

141x101mm (600 x 600 DPI)

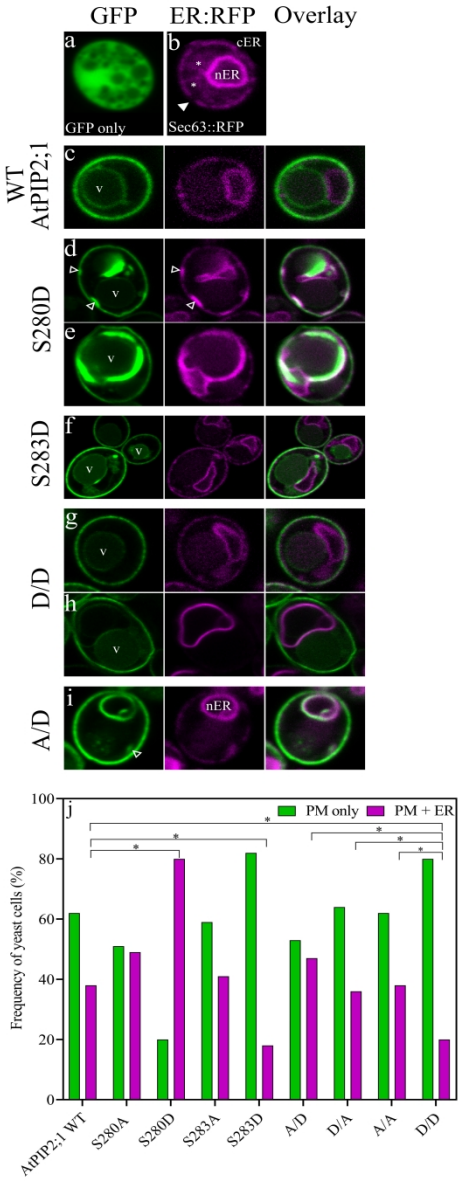

Figure 5: Subcellular localisation of AtPIP2;1 wild-type and S280/S283 phospho-mutants in yeast. (a) GFP control with diffuse cytosolic localised signal. **(b)** SEC63::RFP endoplasmic reticulum marker. The yeast ER network consists of the prominent nuclear envelope ER domain (nER) and a peripheral or cortical ER domain (cER). The cER lies just beneath the plasma membrane but is not continuous around the perimeter with gaps distinguishing it from plasma membrane localisation (solid triangle). Cytoplasmic tubules link the two ER domains (*). **(c)** Wild-type AtPIP2;1::eGFP localises to a distinct continuous ring of expression around the cell perimeter coinciding with the plasma membrane (PM). GFP signal is also weakly present in the tonoplast of the vacuole (V). In this example, no expression is detected in the nER. **(d-e)** The single phospho-mimetic S280D mutant commonly shows a continuous ring of PM localisation along with a substantially stronger GFP signal co-localised with the ER marker in both the peripheral (open arrow heads) and internal ER networks (nER). **(f)** The single phospho-mimetic S283D mutant shows a distinct localisation around the PM with little to no ER co-localisation. Weak GFP signal is occasionally observed in the periphery of the vacuoles (V). **(g-h)** The localisation of the double phosphorylated mimetic D/D mutant occurs almost exclusively in the PM with comparably weak signal

detectable in the tonoplast of the vacuole (V) and little to no signal in the ER. **(i)** The double A/D mutant localises to the PM. Approximately half the yeast cells examined also exhibit strong co-localisation to the ER. **(j)** The frequency of yeast cells with GFP signal detected in the PM only versus co-localisation in both the PM and ER. Asterisks (*) denote statistically significant difference (Fisher's exact test $p \leq 0.05$). N = WtAtPIP2;1(53), S280A(57), S283S(161), S283A(32), S283D(94), A/A(117), D/A(64), A/D(139) , D/D(83).